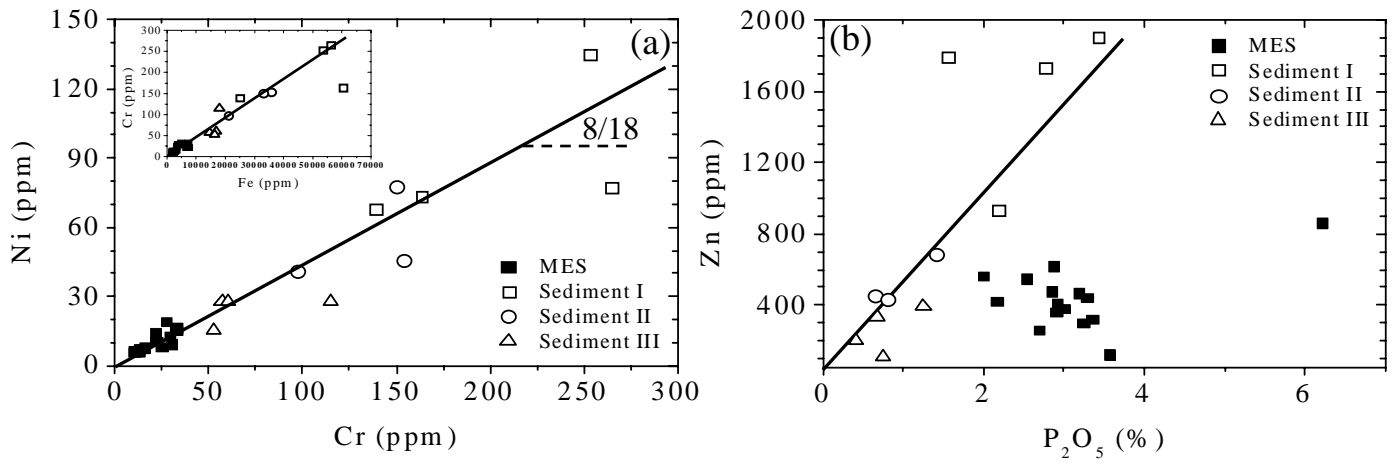
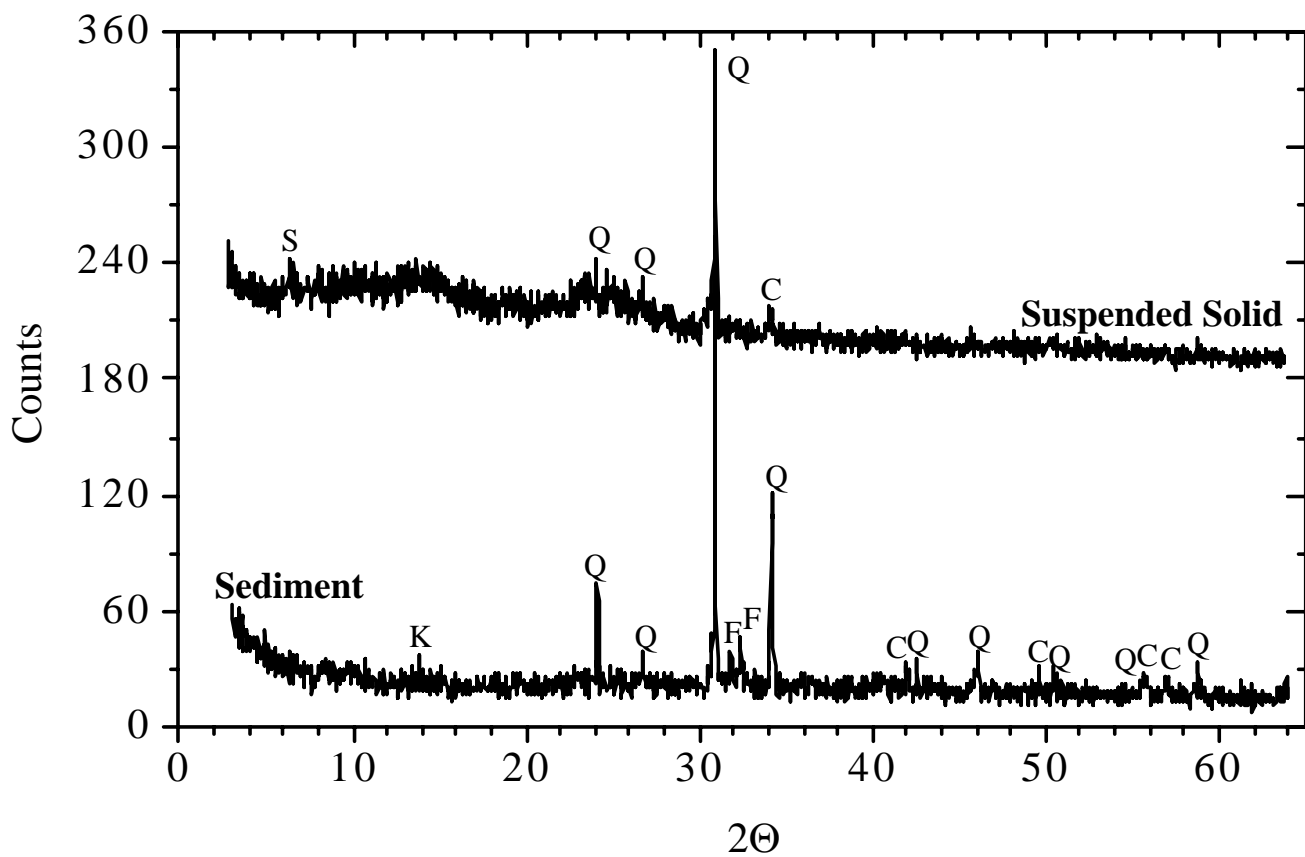


**Figure 1:** (a) Relative percentages of the dissolved and suspended solids phases for Ni, Cr, Cu, Al, Zn, Pb, and Cd, in sewage. The suspended solid phase is shaded.

(b) Dissolved metal concentrations in groundwater, tap water, wastewater, and domestic sewage. See text for the definitions of domestic sewage and wastewater. Error bars correspond to standard deviations to the mean.



**Figure 2:** Relationships between total contents of selected heavy metals: (a) Ni vs Cr and Fe vs Cr (inset); (b) Zn vs P<sub>2</sub>O<sub>5</sub>.



**Figure 3:** Typical X-ray diffractograms of sediment (Fraction I < 50  $\mu\text{m}$  - CL sampling site) and suspended solids (JB sampling site). Q: quartz, C: Calcite, F: Feldspar, K: kaolinite, S: smectite.

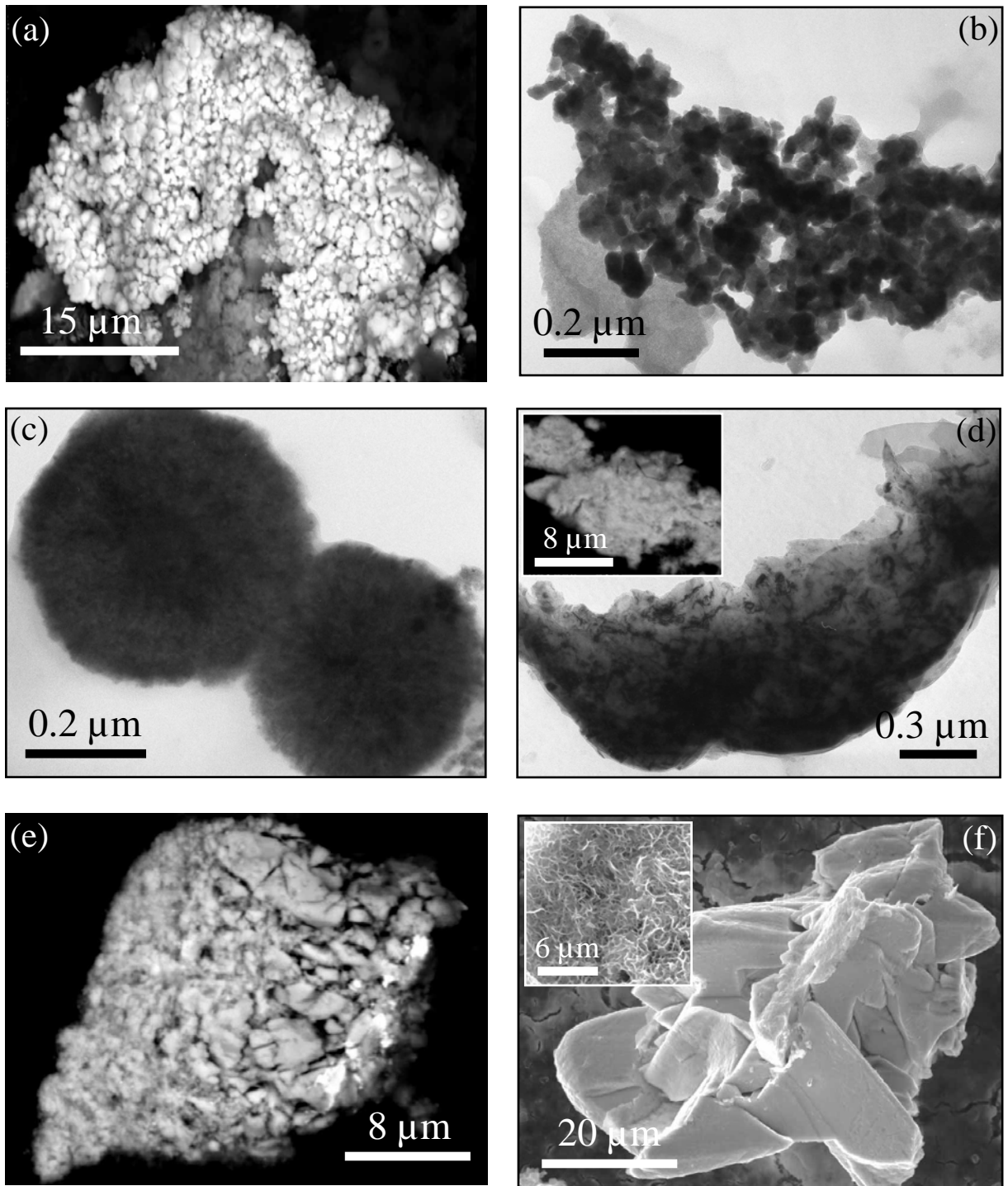


**Figure 4:** Electron micrographs of heavy metal-bearing particles found in sewage suspended solids (a-d) and tap water (e-f and insets d and f). (a) Back-scattered electron image of chalcocite ( $\text{Cu}_2\text{S}$ ); (b) TEM image of copper sulfide  $\text{Cu/S} \sim 1.5$ ; (c) TEM image of sphalerite ( $\text{ZnS}$ ); (d) TEM and BE (inset) images of copper fragments; (e) BEI of corroded soldering material; (f) SEI of hydrocerussite ( $\text{Pb}_3(\text{CO}_3)_2(\text{OH})_2$ ) and BEI of smithonite ( $\text{ZnCO}_3$ ) (inset). The corresponding energy dispersive spectra are provided in supporting information material.

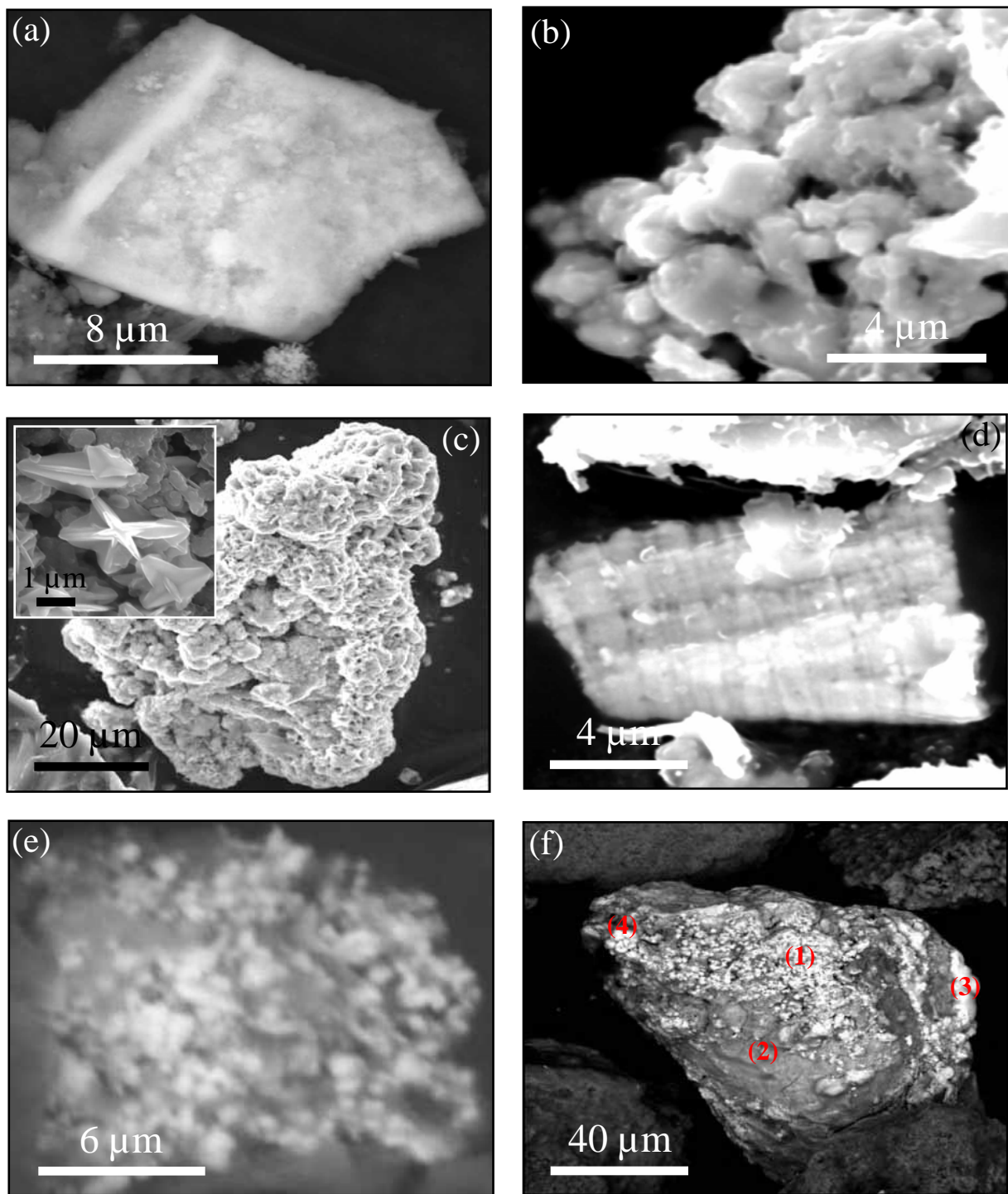


**Figure 5:** Electron micrographs of heavy metal-bearing particles found in sewer sediments. (a) BEI of mackinawite ( $\text{FeS}$ ); (b) BEI of bismuth sulfide; (c) SEI of heterogeneous Cu-Fe-S particle coated with covellite ( $\text{CuS}$ ) (inset); (d) BEI of neoformed galena particle ( $\text{PbS}$ ); (e) BEI of Zn-sulfide grains coating the surface of a barite particle; (f) BEI of partially sulfurized Sn-Pb-Fe-Cu-Zn metal alloy: (1) Lead oxide, (2) Sn-Pb-Fe-Cu alloy, (3)  $\text{SnSO}_4$ , (4)  $\text{PbS}$ . The corresponding energy dispersive spectra are provided in supporting information material.

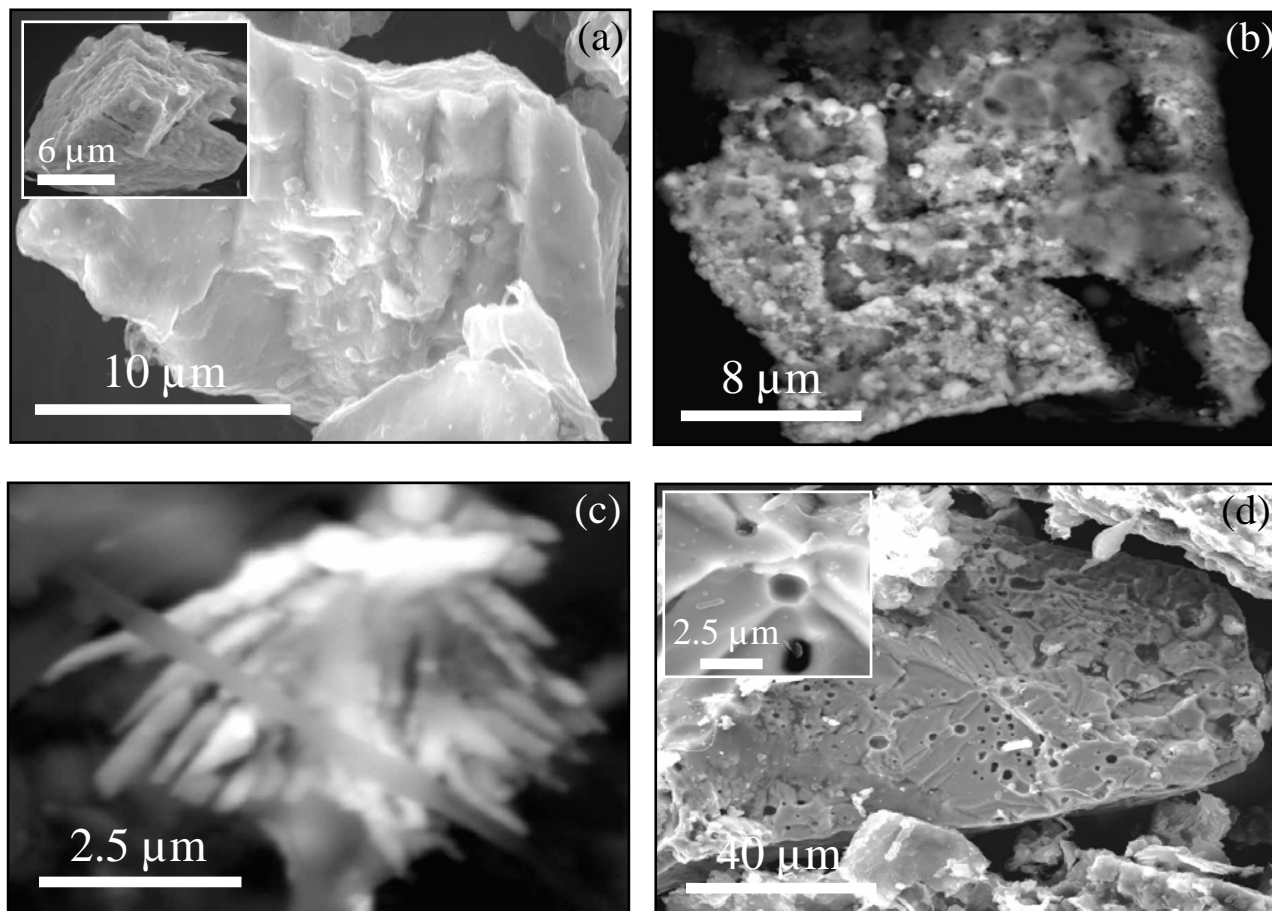


**Figure 6:** Electron micrographs of heavy metal-bearing particles found in sewer biofilms. (a) SEI of sphalerite (ZnS) and galena (PbS) (inset); (b) BEI of a sulfurized Fe-Mn alloy; (c) BEI of a dendritic pyrite particle (FeS<sub>2</sub>); (d) SEI of a microbially-corroded iron oxihydroxide particle - bacteria can be seen within etch pits (inset). The corresponding energy dispersive spectra are provided in supporting information material.

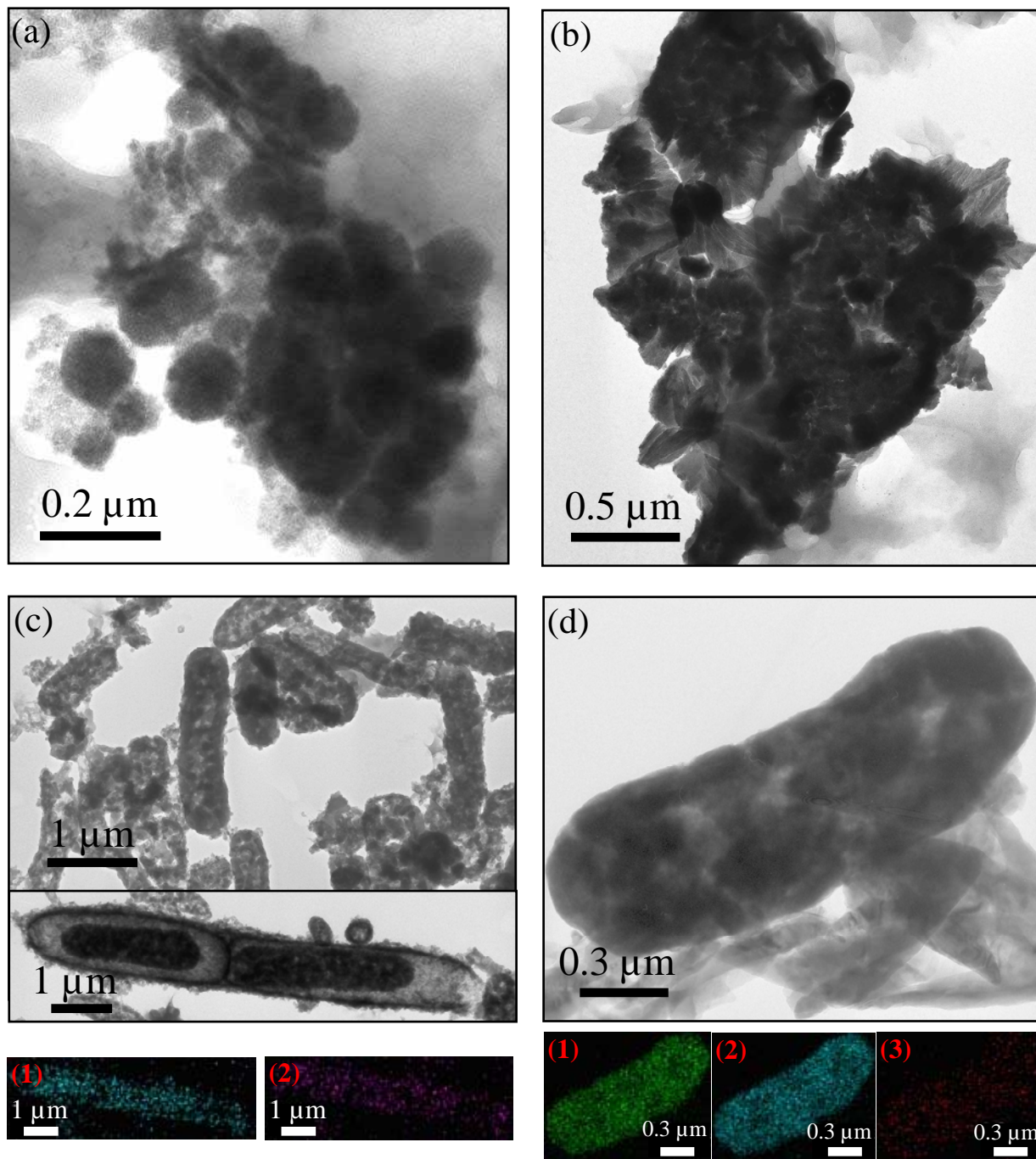


**Figure 7:** TEM images of heavy metal-bearing particles found in washbasin siphon deposits. (a) covellite ( $\text{CuS}$ ); (b) copper sulfide of Cu/S elemental ratio intermediate between chalcocite ( $\text{Cu}_2\text{S}$ ) et covellite ( $\text{CuS}$ ); (c-d) bacteria coated with heavy metal sulfides; TEM elemental mapping of S (c1 and d1), Sn (c2), Zn (d2), and Pb (d3). The corresponding energy dispersive spectra are provided in supporting information material.

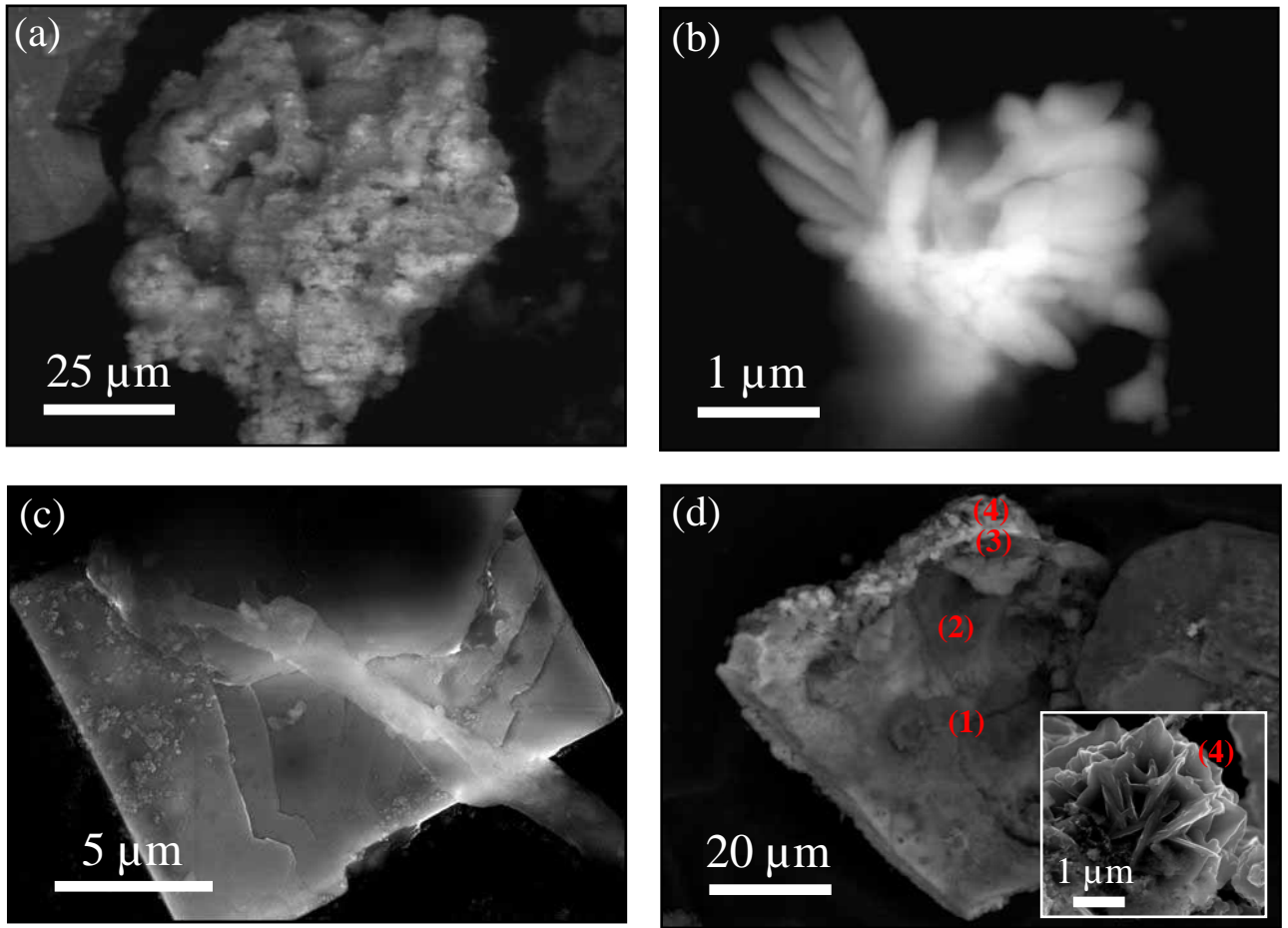


**Figure 8:** SEM-BE images of heavy metal-bearing particles found in sump pit deposits. (a) partially sulfurized cerussite; (b) dendritic chalcocite particle ( $\text{Cu}_2\text{S}$ ); (c) well-crystallized galena ( $\text{PbS}$ ); (d) mixed Cu-Fe sulfide and CuS (inset). The corresponding energy dispersive spectra are provided in supporting information material.